Thermal emittance and response time measurements of negative electron affinity photocathodes

Ivan V. Bazarov,[1,a)] Bruce M. Dunham,[1] Yulin Li,[1] Xianghong Liu,[1] Dimitre G. Ouzounov,[1] Charles K. Sinclair,[1] Fay Hannon,[2] and Tsukasa Miyajima[3]
[1]*Laboratory of Elementary Particle Physics, Cornell University, Ithaca, New York 14853, USA*
[2]*Lancaster University, Lancaster, United Kingdom*
[3]*Photon Factory, KEK, Tsukuba, Japan*

(Received 1 October 2007; accepted 29 November 2007; published online 3 March 2008)

The thermal emittance and temporal response of a photocathode set an upper limit on the maximum achievable electron beam brightness from a photoemission electron source, or photoinjector. We present measurements of these parameters over a broad range of laser wavelength for two different negative electron affinity (NEA) photocathodes. The thermal emittance of NEA GaAs and GaAsP has been measured by two techniques—a measurement of the beam size downstream from a solenoid, whose strength was varied, and a double slit transmission measurement—for different laser spot sizes and shapes. The effect of space charge on the beam spot size allows a good estimation of the photoemission response time from these cathodes. Both cathodes show a subpicosecond response for laser wavelengths shorter than 520 nm. © *2008 American Institute of Physics*. [DOI: 10.1063/1.2838209]

I. INTRODUCTION

Electron linear accelerators (linacs) are known for their ability to preserve a small six-dimensional phase space during acceleration of the beam. The key to a number of applications that utilize linacs is the production of a high brightness, low emittance electron beam. Photoinjectors, which house a photocathode in a high electric field environment, are presently the technology of choice for the generation of low emittance, short (~ps) duration electron bunches. The brightness achievable from a photoinjector results from the interplay of several phenomena: the photoemission process itself, space charge effects in the vicinity of the photocathode, and subsequent beam transport and bunch compression. The emittance growth resulting from the space charge forces acting within a bunch is strongly correlated with longitudinal position in the bunch. This correlated emittance growth can be largely reversed by properly chosen beam optics.[1] By suitably shaping the three-dimensional laser distribution incident on the photocathode,[2,3] the uncorrelated emittance growth can be minimized. The limitations due to the photoemission process itself cannot be removed with electron beam optics, and both the transverse momentum spread and temporal response of the emitted electrons, to the extent that the latter limits the effectiveness of temporal shaping of the laser pulse, are of fundamental importance for low emittance photoinjectors. Recent computational optimizations have shown that it is possible to construct an electron injector based on a very high voltage direct current (dc) photoinjector, in which the final beam emittance is dominated by the thermal emittance from the photocathode.[4] Assuming a very short duration pulse near the cathode, the lowest normalized root-mean square (rms) emittance, $\epsilon_{n,x}$, for a flat-top transverse laser shape illumination is given by

$$\epsilon_{n,x} = \sqrt{\frac{q}{4\pi\epsilon_0 E_{\text{cath}}}\frac{k_B T_\perp}{m_e c^2}}, \tag{1}$$

where q is the bunch charge, $k_B T_\perp$ is the (transverse) beam thermal energy, E_{cath} is the electric field at the cathode, ϵ_0 and $m_e c^2$ are the vacuum permittivity and the electron rest energy, respectively.

In negative electron affinity (NEA) photocathodes, electrons photoexcited into the conduction band of p-type semiconductors rapidly thermalize to the conduction band minimum due to inelastic phonon collisions, and the NEA condition allows these thermalized electrons to escape into vacuum.[5] As a result, the transverse momentum spread can be very low, and the beam (transverse) temperature can approach that of the semiconductor lattice when excited with the photons of near band gap energy. This ability to produce cold beams makes NEA photocathodes appealing for low emittance photoinjectors. The thermal emittance, however, depends on the illuminating wavelength, the degree of negative affinity, and the band structure of the photocathode material. It is also known that photoemission with photons of near band gap energy results in a long temporal tail that extends into the 100 ps range.[6] Such a long response time can render temporal shaping of the laser pulse illuminating the cathode ineffective, increasing the uncorrelated space charge forces acting on the beam and reducing the overall performance of the electron source. The reason for this long response time is that absorption of near band gap energy photons in the semiconductor is relatively low, exciting electrons to the conduction band over a considerable depth in the material, and these electrons must diffuse to the semiconductor surface to be emitted. As the photon absorption in direct band gap semiconductors is a strong function of photon energy, the response time should depend strongly on the wavelength of illuminating light. Finding the optimum wavelength of the laser thus depends on the detailed behavior of

a)Electronic mail: ib38@cornell.edu.

the thermal emittance and photoemission response time with laser wavelength, and represents one of the motivations for the present work.

Several authors have reported thermal emittance or mean transverse energy measurements from NEA GaAs.[7–9] Most of the measurements have been done with near band gap energy photons, and some disagreement with earlier measurements exists. In part, this can be attributed to different NEA cathode preparation techniques, varying electron affinity, and the more general challenge of characterizing beams with very low transverse momentum spread. Likewise, the published results of GaAs photoresponse times are either limited to photon energies near the band gap[6] or inconclusive.[10]

Two different methods, measurement of the transverse beam size downstream of a solenoid lens whose strength is varied, and a direct transverse phase space mapping with double slits, have been applied to measure the thermal emittance of NEA GaAs and GaAsP cathodes in a high voltage dc gun. These measurements have been carried out for a range of wavelengths using multiple laser spot sizes, as well as different transverse profiles. In addition, for the transverse beam size measurements we used two different view screen materials and a wire scanner. We detail our experimental methods for measuring transverse emittance in Sec. II. A new method for inferring photoemission response time from these photocathodes is described in Sec. III. The strong space charge of a bunch produced with a subpicosecond laser pulse will preclude accurate measurements of intrinsic transverse emittance. The same effect, if properly characterized, can be used to infer the photoemission response time by fitting the solenoid scan data with results of particle tracking simulations that include the cathode response time as a fit variable. A convenient analytical expression for the photocathode response function in the context of a diffusion model is provided. Finally, we conclude with a discussion and outlook for the future work.

II. THERMAL EMITTANCE

A. Notations

The normalized rms emittance of the beam in one transverse plane is defined as

$$\epsilon_{n,x} = \frac{1}{m_e c}\sqrt{\langle x^2\rangle\langle p_x^2\rangle - \langle x p_x\rangle^2}, \tag{2}$$

where x and p_x are the transverse position and momentum of an individual particle, and the angular brackets represent the ensemble average of all particles in the beam. A similar definition describes the emittance in the other transverse plane. Introducing the transverse thermal energy of the cathode $k_B T_\perp$, and invoking the equipartition theorem, we write $\frac{1}{2}m_e\langle v_x^2\rangle = \frac{1}{2}k_B T_\perp$ for nonrelativistic photoelectrons, $v_x = p_x/m_e$ being the transverse component of the velocity. The correlation term in Eq. (2) is absent at the photocathode surface, so we write the thermal emittance as

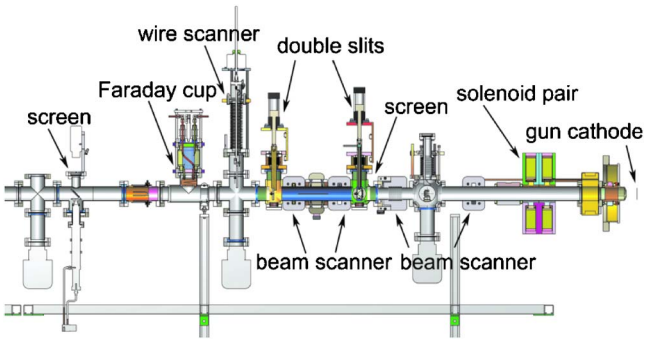

FIG. 1. (Color online) Beam line used in photocathode studies. The beam moves from right to left.

$$\epsilon_{n,x} = \sigma_x\sqrt{\frac{k_B T_\perp}{m_e c^2}}. \tag{3}$$

Here $\sigma_x \equiv \sqrt{\langle x^2\rangle}$ is the rms laser spot size on the cathode.

We use the definition of the cathode thermal energy as given by Eq. (3) throughout this work. Occasionally, more complex formulas have been introduced with the intention of relating photon energy, band gap, and electron affinity to the transverse thermal energy of the cathode assuming the absence of inelastic processes for electrons in the photocathode.[9] As such an assumption may not be satisfied in the photocathodes under study, we chose the simpler definition here. Also, for comparison with other references, note the absence of a factor of 2 next to $k_B T_\perp$ in Eq. (3).

B. Experimental Setup

Cornell University is planning the construction of an ultrabright x-ray light source based on the Energy Recovery Linac (ERL) concept.[11,12] The key component of the ERL is a high average current, low emittance electron injector. To this end, Cornell has an ongoing program to develop a very bright photoinjector system based on high voltage dc gun technology. The measurements reported here were carried out as a part of this program. The dc gun, designed for a 500–750 kV voltage, is equipped with a load-locked photocathode preparation system and operates at a base pressure in the 10^{-12} Torr range. Details on the dc gun can be found elsewhere.[13] To commission the high-voltage dc gun and perform studies of the photocathode properties and space charge dominated beams, a short diagnostics beam line capable of transporting up to 100 mA dc beam current has been assembled. The measurements reported here were mostly done at a gun voltage of 250 kV.

The beam line section directly after the gun is used for the photocathode studies, and is shown in Fig. 1. Two identical solenoids are located back-to-back after the gun. They are wired so that the magnetic field integral is cancelled to avoid rotation of the beam. The beam transverse profile measurements were performed using two different methods: a wire scanner and fluorescent view screens. The wire scanner has a 20 μm gold-plated tungsten wire, which is scanned across the beam by a stepper motor. The current signal from the wire is connected to a trans-impedance amplifier and sampled together with the stepper motor encoder reading at a

500 Hz rate. Two types of view screens, BeO and chemical vapor deposition diamond, were used to observe the beam profile. The optical profiles are measured with a 12-bit charge-coupled device (CCD) camera interfaced to a computer. The beam line is equipped with a double slit emittance measurement system designed for studies of heavily space charge dominated beams. Each slit is 20 μm wide. The first slit is comprised of two parts: a water-cooled guard slit with a 200 μm wide opening, and the actual 20 μm precision slit brazed to it. The function of the guard slit is to intercept most of the beam power, to reduce thermal deformation of the precision slit. This design allows measurements with beam power of up to 1 kW without degradation in performance. Instead of the usual method of stepping the slits through the beam to collect data, the electron beam is moved relative to the slits using two beam scanners, each consisting of a pair of identical air–core correctors of opposite sign. The design and mounting of these correctors assured that quadrupole and sextupole fields were negligible in the region traversed by the beam, as was verified by the beam measurements. A very weak solenoid was located between the two slits to correct for any angular misalignment between them, but in practice, this proved unnecessary. The beam current passing the second slit is measured with an insertable Faraday cup connected to a low-noise current preamplifier. Because of the absence of any moving parts during the scan, a detailed transverse phase space map of the beam may be obtained in less than a minute. The experiment is controlled via EPICS and MATLAB®.

Five different lasers have been used in the photocathode studies. An argon-ion laser provided three different wavelengths: 458, 488, and 514.5 nm. A 5 mW solid-state and a helium–neon laser provided 532 and 633 nm lines, respectively. A Ti:sapphire laser (Mai Tai®, Spectra-Physics) operated below the threshold for pulsing covered the range of 710–870 nm. The same laser operated in the Kerr lens mode-locking regime provided 100 fs full-width at half-maximum (FWHM) pulses at an 80 MHz repetition rate, and was used in the photoemission response studies. By frequency doubling this laser we have also obtained short pulses in the 360–460 nm range. The pulse duration lengthening due to group velocity dispersion in the second harmonic generation crystal is estimated to be less than 300 fs. Finally, a frequency doubled Yb-fiber laser operating at 50 MHz repetition frequency is used for the space charge studies. It has a wavelength of 520 nm and the shortest pulse duration without temporal shaping of 2.5 ps FWHM, as measured by auto-correlation.[14]

A circular aperture illuminated by a laser was 1:1 imaged onto the photocathode, and provided a convenient means of changing the spot size for the thermal emittance measurements. Alternatively, an adjustable telescope was used to relay a Gaussian profile laser beam onto the cathode. For each electron beam data set, the laser beam was diverted after the last lens and the optical profile was viewed with a 10-bit CCD camera at the same distance from the lens as the photocathode. Typical laser spot profiles are shown in Fig. 2 for an imaged circular aperture and the full Gaussian beam after the telescope.

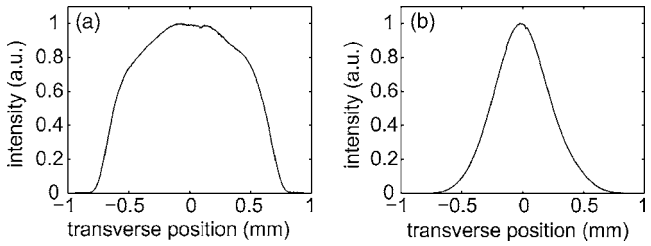

FIG. 2. Typical transverse profile of a laser spot incident on the photocathode (a) after a circular aperture and (b) for a Gaussian imaged beam.

Two cathodes have been used in these studies: GaAs and GaAsP. GaAs wafers with Zn doping between 6.3×10^{18} and 1.9×10^{19} cm^{-3} were activated in the preparation chamber of the load-lock system connected to the gun. A yo-yo preparation with cesium and nitrogen trifluoride gave typical initial quantum efficiencies of 10% at 532 nm. GaAsP photocathodes were activated in a similar fashion. The GaAsP was epitaxially grown by molecular beam epitaxy (MBE) on GaAs substrates to a thickness of 2 μm. The phosphorus concentration was ~45% with a p-doping level of $2-4\times10^{18}$ cm^{-3}. A 2 μm transition layer with graded phosphorus concentration separated the GaAs substrate and the GaAsP active layer to eliminate the strain resulting from the lattice mismatch between GaAs and GaAsP.

C. Method

In the case of decoupled motion and in the absence of space charge and beam dispersion, the n measurements of transverse rms beam sizes $\sigma_x^{(i)}$ at location z_1 corresponding to $i=1,2,\ldots,n$ different optics settings between positions z_0 and z_1 are related to unknown σ-matrix elements $\beta_x\epsilon_x$, $\alpha_x\epsilon_x$, and $\gamma_x\epsilon_x$ at location z_0 by the elements of a 2×2 transfer matrix $\mathbf{R}^{(i)}(z_0\rightarrow z_1)$ for the transverse position and angle as

$$\sum_x = \mathbf{B}_x \mathbf{s}_x. \tag{4}$$

Here the n-component column vector $\Sigma_x \equiv((\sigma_x^{(1)})^2,(\sigma_x^{(2)})^2,\ldots,(\sigma_x^{(n)})^2)^T$, the matrix $\mathbf{B}_x$ of dimension $n\times3$ is given by

$$\mathbf{B}_x \equiv \begin{pmatrix} (R_{11}^{(1)})^2 & 2R_{11}^{(1)}R_{12}^{(1)} & (R_{12}^{(1)})^2 \\ (R_{11}^{(2)})^2 & 2R_{11}^{(2)}R_{12}^{(2)} & (R_{12}^{(2)})^2 \\ \cdots\cdots & \cdots\cdots & \cdots\cdots \\ (R_{11}^{(n)})^2 & 2R_{11}^{(n)}R_{12}^{(n)} & (R_{12}^{(n)})^2 \end{pmatrix}, \tag{5}$$

and the column vector $\mathbf{s}_x \equiv (\beta_x\epsilon_x, -\alpha_x\epsilon_x, \gamma_x\epsilon_x)^T$, where β_x, α_x, and γ_x are Twiss parameters and ϵ_x is the geometric rms emittance, which is related to the normalized emittance by $\epsilon_x = \epsilon_{n,x} m_e c/p_z$, where p_z is the longitudinal momentum.

Introducing normalized quantities $\hat{\Sigma}_x^{(i)} \equiv \Sigma_x^{(i)}/\sigma_{\Sigma_x^{(i)}}$, and $\hat{B}_{x,ij} \equiv B_{x,ij}/\sigma_{\Sigma_x^{(i)}}$, where $j=1$, 2, 3 and $\sigma_{\Sigma_x^{(i)}}$ is the rms error of $\Sigma_x^{(i)} \equiv (\sigma_x^{(i)})^2$, the least-square solution to Eq. (4) is written as[15]

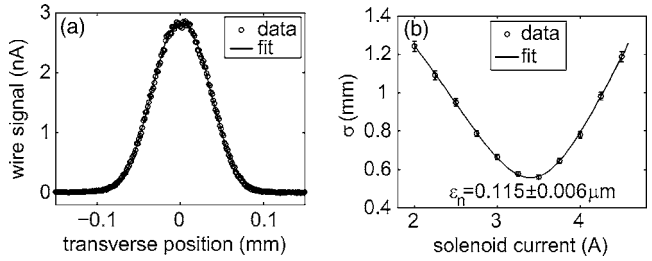

FIG. 3. (a) Typical beam profile as measured by the wire scanner and the fit. (b) Typical solenoid scan data and emittance fit (GaAs, 860 nm).

$$\mathbf{s}_x = \mathbf{T}_x \hat{\mathbf{B}}_x^T \hat{\Sigma}_x, \tag{6}$$

where $n \times n$ covariance matrix $\mathbf{T}_x \equiv (\hat{\mathbf{B}}_x^T \hat{\mathbf{B}}_x)^{-1}$. The error propagation in the emittance measurement, σ_{ϵ_x}, is achieved via

$$\sigma_{\epsilon_x}^2 = (\nabla_{\mathbf{s}_x} \epsilon_x)^T \mathbf{T}_x (\nabla_{\mathbf{s}_x} \epsilon_x), \tag{7}$$

e.g. $\nabla_{\mathbf{s}_x} \epsilon_x = (\gamma_x/2, \alpha_x, \beta_x/2)^T$, where in terms of $\mathbf{s}_x$ elements: $\beta_x = s_{x,1}/\epsilon_x$, $\alpha_x = -s_{x,2}/\epsilon_x$, $\gamma_x = s_{x,3}/\epsilon_x$, and $\epsilon_x = \sqrt{s_{x,1}s_{x,3} - s_{x,2}^2}$.

The transfer matrices were calculated for the actual magnetic field profile of the two back-to-back identical solenoids.[16] Figure 3 shows a typical beam profile as measured by the wire scanner, a solenoid scan data set, and the fit. Most thermal emittance measurements were carried out at 250 kV gun voltage with a dc beam of ~1 μA, making space charge effects inconsequential. A cross check for the measured emittance was carried out at 200 and 250 kV, yielding the same normalized emittance within 1%.

All beam profile data taken with the wire scanner or the screen were fitted with a super-Gaussian $y = Ae^{-|x-x_0|^m/w^m} + B$ with free parameters A, B, m, w, and x_0. The rms beam size is given by $w\sqrt{\Gamma(3/m)/\Gamma(1/m)}$. This family of curves provides a better fit than a simple Gaussian to the measured electron beam profiles obtained for non-Gaussian laser spots on the cathode. The largest measurement uncertainty in determining the beam size is estimated to be 2%. The measurement uncertainty was propagated in a χ^2 fit to the emittance according to the Eq. (6). Typical errors on the emittance add up to 4% for the wire scanner and 5% for the view screen measurements. The thermal energy was determined from the slope of a line passing through the origin and χ^2 fitted to the emittance versus the laser spot size.

The double slit measurement provides a full map of the transverse phase space. Figure 4 shows typical transverse phase space maps for both cathode types obtained by the double slit measurements. Noise and background subtraction are important when calculating the rms emittance using two-dimensional intensity maps. We employ a self-consistent, unbiased rms emittance analysis (SCUBEEx).[17] In this method, an ellipse that contains the data is varied in size. The regions outside of the ellipse are treated as noise, and its average value is subtracted from the whole data. The rms emittance is calculated as a function of the encompassing ellipse area. When the ellipse is large enough to include the full beam, the calculated emittance should not depend on its size assuming the noise is uncorrelated in nature, and the value so found represents the 100% rms emittance. Figures 4(c) and 4(d) show the output from SCUBEEx analysis of the data shown in Figs. 4(a) and 4(b), respectively.

To establish confidence in the emittance measurement procedure, we have performed a crosscheck of the different measurement techniques: a solenoid scan using both a view screen and the wire scanner, and the direct transverse phase space mapping with double slits. Measurements taken with different laser spot sizes and profiles are shown in Fig. 5. Most of remaining thermal emittance measurements reported here are made using the wire scanner and solenoid scan method.

D. Results

Figure 6 shows the thermal emittance measurements for GaAs. The typical quantum efficiency (QE) is approximately 5% at 532 nm for these measurements. We have observed some changes in the cathode thermal energy due to varying

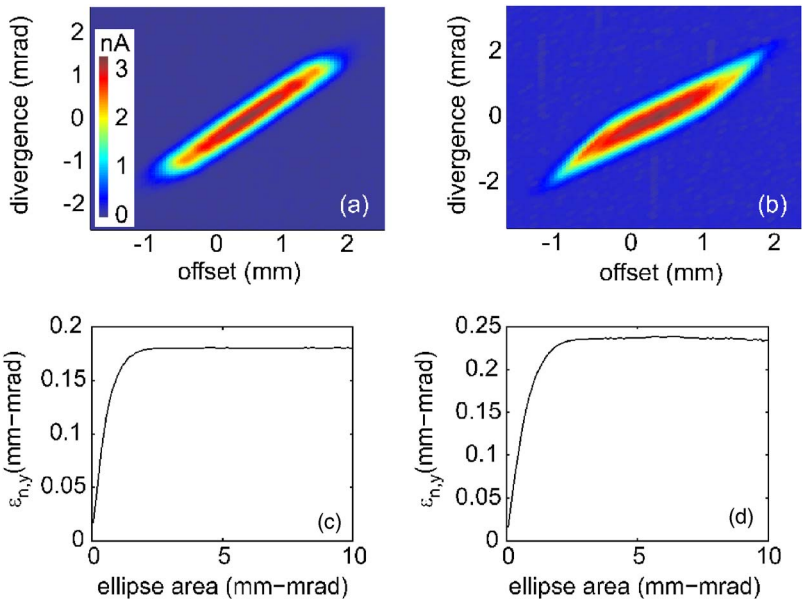

FIG. 4. (Color online) Transverse phase space of the beam with thermal emittance. Current signal in nA. (a) GaAs and (b) GaAsP. Calculated emittances as a function of encompassing ellipse area after the noise subtraction for (c) GaAs and (d) GaAsP data, respectively (refer to the text).

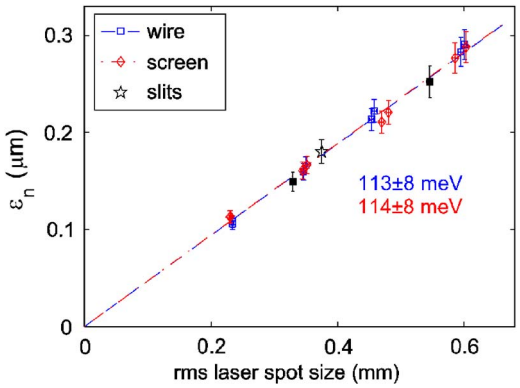

FIG. 5. (Color online) Comparison between different emittance measurement techniques for GaAs at 532 nm. Filled squares correspond to a Gaussian laser profile.

QE for GaAs and more noticeably for GaAsP. Figure 7 shows the thermal emittance measurements for GaAsP at different wavelengths and for 1% and 6% QE. The change in the thermal energy is outside of the measurement error and is thought to be due to varying surface conditions, and in particular, the value of NEA. Figure 8 summarizes the dependence of the transverse thermal energy of GaAs for different laser wavelengths. The data in the 710–865 nm range was taken with a single aperture of 1.5 mm diameter using the Ti:sapphire laser. Figure 9 shows the transverse thermal energy of GaAsP for laser wavelengths between 460 and 633 nm.

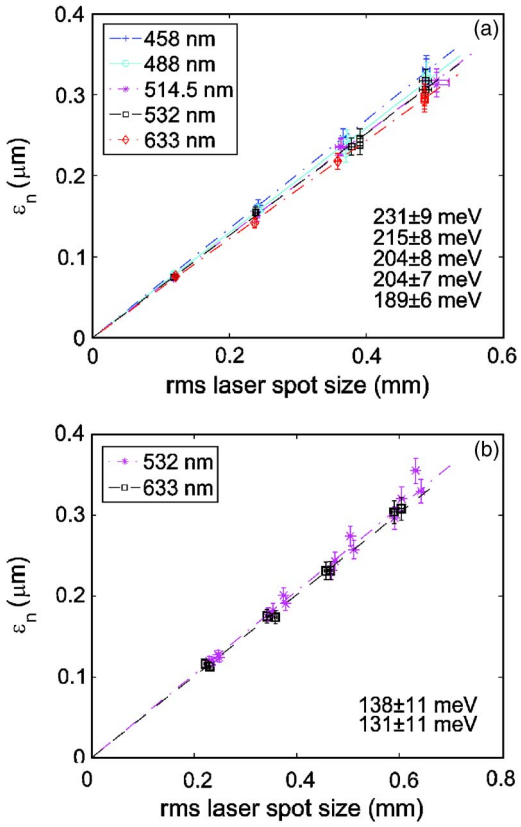

FIG. 7. (Color online) Thermal emittance of GaAsP as a function of rms laser spot size. (a) QE=6% and (b) QE=1%.

III. PHOTOEMISSION RESPONSE

A. Diffusion model

Following the three-step model of photoemission,[18] a diffusion model has been used to explain the measured photoemission temporal response curves from GaAs illuminated by near band gap energy photons.[6] Although the value for the diffusion coefficient obtained from fitting the data differed from published values for heavily *p*-doped material, this theoretical model was able to reproduce the measured temporal response profiles extremely well. In this section we will provide a convenient analytical form of the photoemission response function in the framework of this theory. Assuming that the temporal distribution of the photoemitted electrons is dominated by electron diffusion over the full range of wavelengths available to us, we were able to infer the photocathode response time from beam size measurements in our well-characterized beam line by comparing them to simulations of the space charge effect in case of a tightly focused laser spot and electron bunches of about 100 fC charge.

Following Ref. 6, we solve the simplified diffusion equation for the electron concentration, $c(h,t)$, in the bulk of the photocathode after excitation from a delta-function laser pulse arriving at $t=0$:

$$\frac{\partial c(h,t)}{\partial t} = D\frac{\partial^2 c(h,t)}{\partial h^2}. \tag{8}$$

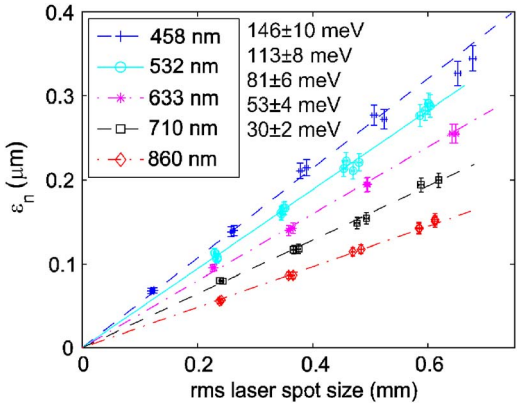

FIG. 6. (Color online) Thermal emittance of GaAs as a function of rms laser spot size for various illumination wavelengths.

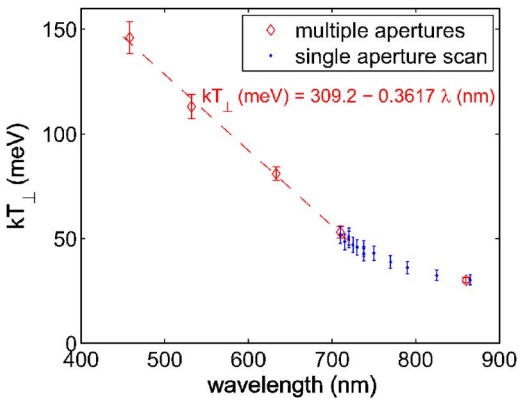

FIG. 8. (Color online) Thermal energy of GaAs as a function laser wavelength.

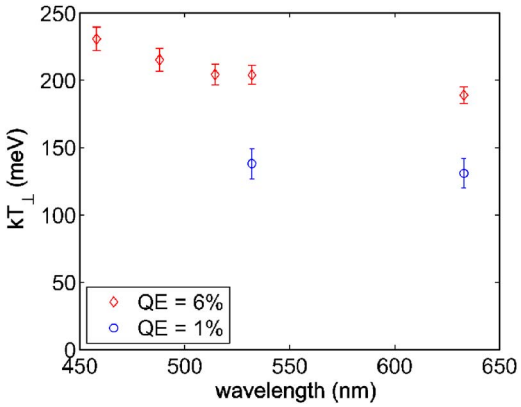

FIG. 9. (Color online) Thermal energy of GaAsP as a function laser wavelength.

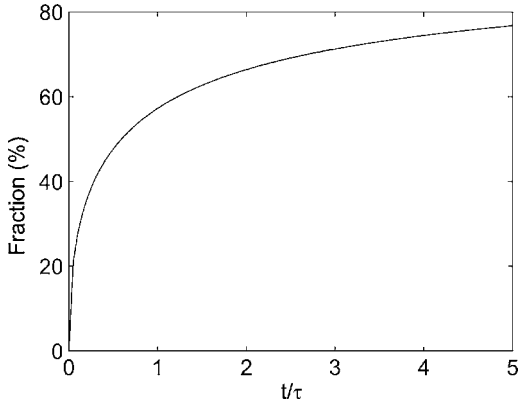

FIG. 10. Fraction of the electron pulse emitted up to time t upon arrival of a delta-function laser pulse for the photoemission response function given by Eq. (11).

The following initial and boundary conditions apply: $c(h,t=0)=c_0e^{-\alpha h}$ and $c(h=0,t)=0$. Here, D is the electron diffusion constant and α is the optical absorption coefficient. The problem is treated as a one-dimensional transport problem, with h being the spatial coordinate perpendicular to the cathode surface. Additional approximations leading to Eq. (8) include neglecting electron recombination due to its very long time scale compared to the emission process, and ignoring the time for the laser pulse to travel inside the photocathode material (fs scale). The boundary condition $c(h=0,t)=0$ reflects the NEA nature of the surface, whereas the actual photoemission current is proportional to

$$I(t) \propto \frac{\partial}{\partial t}\int_0^\infty c(h,t)dh. \tag{9}$$

Here we assume a crystal thickness that is very large compared to α^{-1}.

The problem has an exact analytical solution for the photoemission current, which is given by

$$I(\kappa) \propto \frac{1}{\sqrt{\pi\kappa}} - \exp(\kappa)\mathrm{erfc}(\sqrt{\kappa}) \tag{10}$$

with normalized time $\kappa \equiv t/\tau$, where $\tau \equiv \alpha^{-2}D^{-1}$, and $\mathrm{erfc}(\xi)$ being the complementary error function $\mathrm{erfc}(\xi) \equiv (2/\sqrt{\pi})\int_\xi^\infty e^{-\zeta^2}d\zeta$. The function is singular at $t=0$, and the actual temporal response profile is given by the convolution of the laser pulse with the profile given by Eq. (10). The fraction of the pulse $P(\kappa)$ emitted up to time $t=\kappa\tau$ from the arrival of a delta-function laser pulse is given by

$$P(\kappa) = 1 - \exp(\kappa)\mathrm{erfc}(\sqrt{\kappa}). \tag{11}$$

A plot of $P(t)$ versus time in units of τ is shown in Fig. 10. The response is characterized by both a very fast component as well as a relatively long tail. The characteristic time τ corresponds to photoemission of 57% of the pulse, whereas 10τ corresponds to 83%.

B. Method

Conventional measurements of the photoemission response time typically require a transverse deflecting rf structure to produce a streak-camera action relating arrival time to transverse displacement, and a well-synchronized laser providing ultrashort pulses. Accurate temporal measurements with picosecond resolution are not routine. Here we propose and demonstrate a new technique which relies on using the space charge effect. Figure 11 presents beam-tracking simulations that illustrate the basic principle. A tightly focused (0.12 mm rms) laser spot produces short electron bunches of known charge. The beam size evolves under the influence of the external electromagnetic fields, as well as the internal

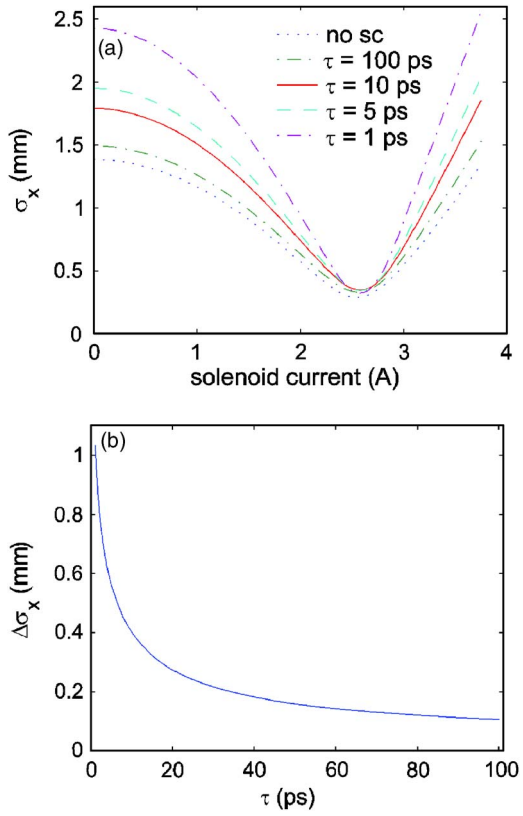

FIG. 11. (Color online) Calculated dependence of the transverse beam size of the beam at the location of the wire scanner for different values of parameter τ. Charge per bunch 100 fC, gun voltage 250 kV, $k_BT_\perp$ 150 meV, initial rms laser spot size 120 μm. (a) Solenoid scan and (b) change of the spot size relative to the case of negligible space charge for unpowered solenoid as a function of parameter τ.

TABLE I. Results of data fitting for GaAs response time.

Wavelength (nm)	τ(ps)	Comment
860	76 ± 26	$V_{gun}=200$ kV
860	69 ± 22	$V_{gun}=250$ kV
785	11.5 ± 1.2	$V_{gun}=200$ kV
785	9.3 ± 1.1	$V_{gun}=250$ kV
710	5.8 ± 0.5	$V_{gun}=200$ kV
710	5.2 ± 0.5	$V_{gun}=250$ kV
520	≤ 1	Upper estimate placed
460	≤ 0.14	Upper estimate placed

space charge forces. The transverse space charge force is proportional to the peak current, which in turn is related to the bunch duration. Figure 11(a) shows the space charge calculations for a bunch emitted from the photocathode, and transported through the gun and solenoid to the wire scanner located 1.790 m from the cathode using the space charge code ASTRA.[19] The fields in the gun and solenoid were calculated using the static field finite element solver POISSON.[20] The magnetic field profile of the solenoids has been measured and found to be in excellent agreement with the calculations.[16] Figure 11(b) shows the sensitivity of the spot size at the wire scanner on the parameter τ for a 100 fC bunch and with the solenoids unpowered. As it is possible to measure changes in the rms transverse beam size as small as tens of μm, the method is quite sensitive to the photoemission response time, especially for prompt emitters. A great advantage of this technique is that the rf deflecting structure and synchronized laser are not required. The disadvantage is the required assumption of the initial temporal profile shape.

The measurements were carried out as follows. Solenoid scans of the electron beam size were performed with short laser pulses providing approximately 100 fC bunches at two different voltages, 200 and 250 kV. The laser was operated either continuous wave (giving a negligible space charge), or with a very short duration, small bunch charge. The measured laser transverse profile was used to generate a quasi-random initial electron distribution for the space charge code. The data in the case of negligible space charge forces were χ^2-fitted using the beam tracking code with space charge forces turned off to find $k_B T_\perp$. The thermal cathode energy so found was consistent with measurements reported in the previous section. This value was then inserted into the code for the χ^2 fit to the data with 100 fC per bunch, where the fit could then be made with only one free variable, τ. The initial temporal distribution was found by convolution of the known laser pulse duration with the photoemission response as given by the Eq. (10). To resolve the fine features of the photoemission temporal profile, the longitudinal space charge mesh size was specified to be 200. The agreement in the value of τ obtained for different gun voltages indicates the consistency of the method.

C. Results

The results are summarized in Tables I and II. Figure 12 shows a fit of the measured data in the case of GaAs excited by 100 fs laser pulses for two different gun voltages. The good agreement between the two values strongly supports the validity of the method. The rather large uncertainty in τ for GaAs at 860 nm is primarily due to the poor sensitivity of the method for very long response times, as shown in Fig. 11(b). We note that the GaAs response time so determined is in reasonable agreement with previous rf deflection measurements with near band gap energy photons.[6]

TABLE II. Results of data fitting for GaAsP response time.

Wavelength (nm)	τ(ps)	Comment
520	≤ 1	Upper estimate placed
400	≤ 0.14	Upper estimate placed

In the case of 520 nm for both GaAs and GaAsP, and 460 nm for GaAs and 400 nm for GaAsP, the fitted response could only be assigned an upper limit. In all these cases, excellent fits to the data were possible by assigning the initial temporal electron distribution to follow the known laser pulse duration exactly, as shown in Fig. 13. For these cases we estimate $\tau \leq 0.14$ ps for 400 and 460 nm, and $\tau \leq 1$ ps for 520 nm.

IV. DISCUSSION

The measured thermal emittances for NEA GaAs are in a good agreement with the previous measurements of Ref. 7, whereas in noticeable disagreement with Ref. 9. In particular, we find the rms normalized emittance from GaAs when excited with 860 nm light is as small as 0.121 ± 0.004 mm mrad for a 1 mm radius uniform laser

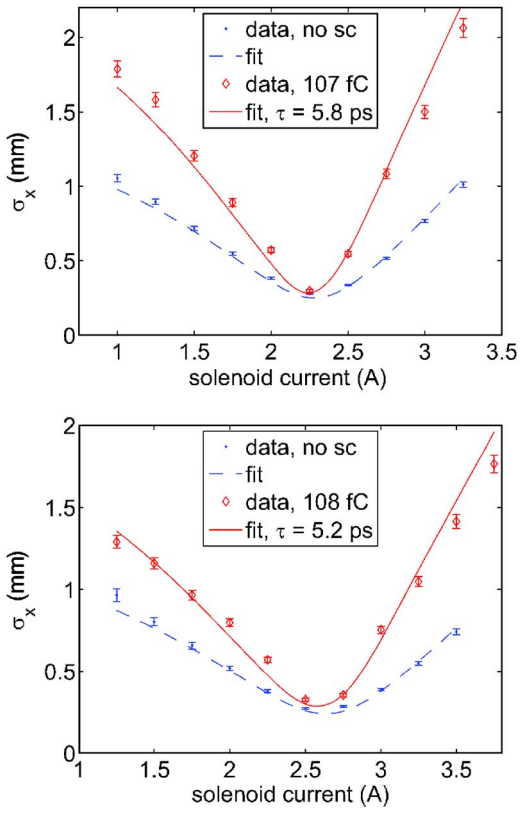

FIG. 12. (Color online) Fit of the measured solenoid scan when excited by 100 fs laser pulse at 710 nm. (a) 200 kV and (b) 250 kV.

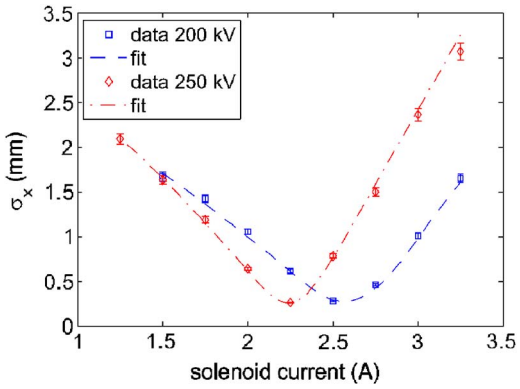

FIG. 13. (Color online) Example of fit to solenoid scan data for GaAs when excited with 300 fs laser pulses at 460 nm. The bunch charge is 97 fC, the initial electron distribution is assumed to be identical to the laser (prompt response). All parameters except for the gun voltage are identical for the two fitted curves.

spot illumination. We note the absence of emittance measurements for different laser spot sizes, and the reliance on a single measurement technique in Ref. 9.

The measured transverse thermal cathode energy for GaAsP is consistently higher than that of the bulk GaAs despite the fact that the band gap of GaAsP, which undergoes a transition from direct to indirect gap for 45% phosphorus concentration, is more closely matched to the shorter laser wavelength than GaAs. The larger $k_B T_\perp$ obtained from GaAsP photocathodes is consistent with previous measurements of the energy spectra of emitted electrons using a parallel-plate geometry.[21] The authors in that reference suggest a larger amount of scattering before emission to be the cause. Their speculation is that this is due to a wider band-bending region, caused by increased NEA, as well as greatly increased intervalley scattering due to the high-mass X and L valleys being closer to the Γ valley in comparison with GaAs. Nevertheless, the detailed mechanism for the higher energy spread is not understood.

The measured photoemission response from the two NEA photocathodes displays a very strong dependence on the laser wavelength. This is not surprising given that the absorption in GaAs changes by more than an order of magnitude over the range of wavelengths under study. Thus, the expected and observed change in the response time is over two orders of magnitude.

In the future, we plan to conduct detailed studies of the temporal profile of emitted electrons from GaAs and GaAsP at 520 nm wavelength using a deflecting rf cavity.

V. SUMMARY

By measuring one of the important parameters for advanced accelerator applications of the photocathodes, namely, the thermal emittance, we have evaluated the potential of NEA photocathodes for very high brightness beam production. The space charge effect in short bunches has allowed us to deduce the temporal response time of these photocathodes. Both GaAs and GaAsP are found to be prompt emitters (<ps) for wavelengths less than 520 nm. The information on the cathode thermal energy and the response time will aid the optimal choice of laser wavelength for various photoinjector designs utilizing low emittance NEA photocathodes.

ACKNOWLEDGMENTS

This work is supported by the NSF Grant No. PHY-0131508 and NSF/NIH-NIGMS Award No. DMR-0225180.

[1] B. E. Carlsten, Nucl. Instrum. Methods Phys. Res. A **285**, 313 (1989).
[2] H. Tomizawa, H. Dewa, T. Taniuchi, A. Mizuno, T. Asaka, K. Yanagida, S. Suzuki, T. Kobayashi, and H. Hanaki, in Proceedings of the 2002 European Particle Accelerator Conference, Paris, 2002, p. 1819.
[3] J. Yang, F. Sakai, T. Yanagida, M. Yorozu, Y. Okada, T. Nakajyo, K. Takasago, and A. Endo, in Proceedings of the 2002 European Particle Accelerator Conference, Paris, 2002, p. 1828.
[4] I. V. Bazarov and C. K. Sinclair, Phys. Rev. ST Accel. Beams **8**, 034202 (2005).
[5] J. I. Pankove, *Optical Processes in Semiconductors* (Prentice-Hall, Englewood Cliffs, NJ, 1971).
[6] P. Hartmann, J. Bermuth, D. v. Harrach, J. Hoffmann, S. Kbis, E. Reichert, K. Aulenbacher, J. Schuler, and M. Steigerwald, J. Appl. Phys. **86**, 2245 (1999).
[7] B. M. Dunham, L. S. Cardman, and C. K. Sinclair, in Proceedings of the 1995 Particle Accelerator Conference, Dallas, TX, 1995, p. 1030.
[8] S. Pastuszka, M. Hoppe, D. Kratzmann, D. Schwalm, A. Wolf, A. S. Jaroshevich, S. N. Kosolobov, D. A. Orlov, and A. S. Terekhov, J. Appl. Phys. **88**, 6788 (2000).
[9] N. Yamamoto, M. Yamamoto, M. Kuwahara, R. Sakai, T. Morino, K. Tamagaki, A. Mano, A. Utsu, S. Okumi, T. Nakanishi, M. Kuriki, C. Bo, T. Ujihara, and Y. Takeda, J. Appl. Phys. **102**, 024904 (2007).
[10] A. V. Aleksandrov, M. S. Avilov, R. Calabrese, G. Ciullo, N. S. Dikansky, V. Guidi, G. Lamanna, P. Lenisa, P. V. Logachov, A. V. Novokhatsky, L. Tecchio, and B. Yang, Phys. Rev. E **51**, 1449 (1995).
[11] CHESS Technical Memo 02–003, JLAB-ACT-01–04, edited by S. M. Gruner and M. Tigner, Cornell University, 2001.
[12] I. V. Bazarov, D. H. Bilderback, S. M. Gruner, H. S. Padamsee, R. Talman, M. Tigner, G. A. Krafft, L. Merminga, and C. K. Sinclair, in Proceedings of the 2001 Particle Accelerator Conference, Chicago, IL, 2001, p. 230.
[13] B. M. Dunham, C. K. Sinclair, I. V. Bazarov, Y. Li, X. Liu, and K. W. Smolenski, in Proceedings of the 2007 Particle Accelerator Conference, Albuquerque, NM, 2007, p. 1224.
[14] D. G. Ouzounov, I. V. Bazarov, B. M. Dunham, C. K. Sinclair, S. Zhou, and F. Wise, in Proceedings of the 2007 Particle Accelerator Conference, Albuquerque, NM, 2007, p. 530.
[15] M. G. Minty and F. Zimmermann, *Measurement and Control of Charged Particle Beams* (Springer, New York, 2003).
[16] I. V. Bazarov, B. M. Dunham, F. Hannon, Y. Li, X. Liu, T. Miyajima, D. G. Ouzounov, and C. K. Sinclair, in Proceedings of the 2007 Particle Accelerator Conference, Albuquerque, NM, 2007, p. 1221.
[17] M. P. Stockli, R. F. Welton, and R. Keller, Rev. Sci. Instrum. **75**, 1646 (2004).
[18] W. E. Spicer, Phys. Rev. **112**, 114 (1958).
[19] K. Flottmann, Astra—a space charge tracking algorithm, available at http://www.desy.de/~mpyflo.
[20] J. Billen and L. Young, Report No. LA-UR-96–1834, Los Alamos Laboratory Technical, 2000.
[21] A. W. Baum, W. E. Spicer, R. F. Pease, K. A. Kostello, and V. W. Aebi, Proc. SPIE **2550**, 189 (1995).